On the Use of Adjoint Methods for Refractivity Estimation in the Troposphere

Uygar Karabaş, Youssef Diouane, Rémi Douvenot

On the Use of Adjoint Methods for Refractivity Estimation in the Troposphere

Uygar Karabaş*,†, Youssef Diouane*, Rémi Douvenot†,
*ISAE-SUPAERO, Université de Toulouse, 31400 Toulouse, France.
†ENAC, TELECOM, Université de Toulouse, 31400 Toulouse, France.
uygar.karabas@enac.fr

***Abstract*—This paper presents a preliminary study of a new inversion strategy combining the method of adjoint applied to the wide-angle parabolic equation and the method of split-step wavelet for tropospheric refractivity estimation. Our main motivation is to use a gradient based optimization method to infer atmosphere from radio-frequency data, in an effort towards a real-time accurate refractivity-from-clutter system. The proposed adjoint formulation is validated with the method of finite differences. The validation setup is developed for inversion using a tomographic approach.**

***Index Terms*—Inverse Problems; Troposphere Propagation; Adjoint Method.**

I. Introduction

The prediction of the refractive index distribution in the lower troposphere is fundamental for estimating the performance of communication and surveillance platforms operating in maritime environment. Dynamic nature of the lower troposphere poses a challenge for conventional methods of obtaining the refractivity with difficult-to-deploy expensive equipments. The advantage of inferring refractivity from clutter (RFC) (e.g., [1], [2], [3]) is the real-time sensing of the environment within extended range for extended duration with a radar only. Ongoing research in RFC aims at developing a real-time accurate method of inversion (e.g., [4]).

Historically, the inversion methods which have been used in the RFC community adopt parabolic equation (PE) solved with split-step Fourier (SSF) technique [5]. They generally require lots of forward model simulations, hence problems with low-dimensional parameter vector are considered [3]. Zhao *et al.* [6] have demonstrated the applicability of the method of adjoint for RFC when high-dimensional problem is accounted for. In their work, narrow-angle approximation of PE (NAPE) has been solved with SSF applying a tomographic approach.

In this work, a new adjoint formulation is developed in order to tackle high-dimensional problems. In this context, our aim is to use a gradient based optimization method to infer atmosphere from radio-frequency (RF) data, in an effort towards a real-time accurate RFC system. Adjoint methods are known for their accuracy and rapidity to estimate the gradient. Inversion accuracy can be further improved by considering a wave equation which is more accurate than NAPE in realistic scenarios. In accordance with the forward model, the adjoint model can be derived directly from the one-way wave equation and can be approximated in a second time (e.g., to wide-angle PE (WAPE)). Rapidity of inversion can be further improved by adopting the numerical solution of WAPE for both forward and adjoint models from split-step wavelet (SSW) [7] which outperforms SSF in terms of computational time. Consequent RFC system computes the gradient at the cost of two inexpensive SSW runs only, regardless of the number of parameters to invert.

The major contribution of this paper is to propose an approximate adjoint model to the one-way equation. Then the inexpensive SSW method is used for computing both direct and adjoint fields. The new inversion strategy is validated with finite differences (FD), which lacks in the previous works.

The outline of this paper is as follows. Firstly, the forward model is introduced in Section II. The cost function, adjoint model and the gradient are formulated in Section III. The computational setup is detailed in Section IV-A. The justifications for the choice of computational setup are found in Section IV-B with details of the validation strategy. Numerical results for validation are presented in Section IV-C for evaluation of the gradient. Finally inversion results are discussed in Section IV-D.

II. Forward Model

There are several choices to model the electromagnetic wave propagation in the lower troposphere. This paper considers the one-way equation, which is the forward propagating part of the Helmholtz equation in cylindrical coordinates, as the forward model [5]:

$$\partial_r u - jk_0\left(1-Q\right)u = 0, \tag{1a}$$

$$u(r,0) = 0, \tag{1b}$$

$$u(0,z) = \phi(z), \tag{1c}$$

which is numerically solved using SSW [7]. Operator Q is given by $Q = \sqrt{k_0^{-2}\partial_z^2 + m^2(z)}$. Field $u(r,z) \in \mathbb{C}$ is related to the electric or magnetic field propagating at frequency $f = k_0/2\pi$ through a medium with refractive index $n(z)$ and $m(z) = n(z) + z/r_{earth}$ is the refractivity for flattened-earth approximation, with r_{earth} being the radius of earth.

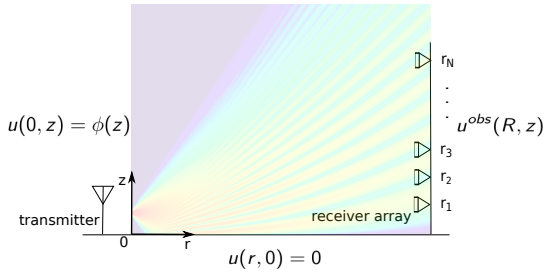

Fig. 1. Schematic of the bistatic configuration.

III. Adjoint Model

A. Cost Function

Let the function $u \in \mathcal{L}^2(\Omega)$ in domain $\Omega = [0, R] \times [0, Z]$. Consider the setup of the tomographic approach which is schematized in Fig. 1. For samplings on u obtained at $(r, z) = (R, z)$, the observed field is denoted by $u^{obs}(R, z)$ and its simulated counterpart is denoted by $u_m(R, z)$. The misfit between the simulation and the observation is estimated as:

$$J(m) = \frac{1}{2} \int_0^Z |u_m(R, z) - u^{obs}(R, z)|^2 dz. \tag{2}$$

The function u_m is solution of (1) using the refractivity model m.

B. Adjoint Model

The variational form is obtained when tangent-linear model of the parabolic equation (1) is multiplied by $w(r, z) \in \mathbb{C}$ and integrated on the domain Ω [8]. The adjoint model (AM) is:

$$\partial_r w - jk_0 \left(1 - Q^*\right) w = 0, \tag{3a}$$
$$w(R, z) = u_m(R, z) - u^{obs}(R, z), \tag{3b}$$
$$w(r, 0) = 0, \tag{3c}$$

where w is obtained by solving (3) in opposite direction to (1). The gradient of the cost function is estimated as:

$$\nabla_m J = k_0 m \int_0^R \Re \left\{ j \left[Q^{-1}\right]^* \overline{u_m} \cdot w \right\} \, dr, \tag{4}$$

where the operator Q^{-1} denotes the inverse of the operator Q and the superscript * denotes its adjoint. $\Re\{x\}$ denotes the real part of $x \in \mathbb{C}$.

IV. Numerical Analysis

In the context of this paper, we use the steepest descent optimization method for the inversion. Therefore the validation of the gradient is crucial. The optimization employs the gradient computed with AM. One classical way of validating the gradient $\nabla_m J_{AM}$ obtained from AM is to compare it to the gradient estimated with FD, denoted by $\nabla_m J_{FD}$. Although FD is expensive and gives only a numerical approximation of the gradient computed with AM, comparison with FD is still useful for validation purpose [8].

A. Computational Setup

The discretized domain Ω_{N_r, N_z}, where N_r and N_z are the number of discretizations along the respective indices, has the size of $R = 100$ m and $Z = 150$ m. The domain is discretized with a uniform grid with the cell size of $\Delta r = \Delta z = 1$ m. The initial condition $\phi(z)$ is given by the complex-point source positioned at $(r_s, z_s) = (-100 \text{ km}, 25 \text{ m})$ with width of 5 m and radiation frequency of $f_s = 2$ GHz at horizontal polarization. Note that $\phi(z)$ is almost a plane wave.

The variation of the refractivity m in the lower troposphere is typically between 1.00025-1.0004 [1]. It is customary to describe refractivity via modified refractivity M given by $M(z) = (m(z) - 1) \times 10^6$. The objective and the initial modified refractivity parameters of the computational setup are given in Fig. 2 and they are respectively denoted by M_{opt} and M_0. The initial guess M_0 is constant refractivity: $M_0(z) = 330$ M-unit. The parameter M_{opt} is composed of three line segments, each described with the segment thickness t and slope s. From $z = 0$ to $z = Z$, the parameters of the objective refractivity are $t = \{50, 50, 50\}$ m and $s = \{0.4, -0.4, 0.118\}$ M-unit/m. There is no variation of refractivity with range. The simulations estimate the refractivity model m from the two parametric distibutions (initial and objective) at grid nodes, i.e., $m \in \mathbb{R}^{N_z}$. Consequently, we invert $N_z = 150$ refractivity parameters.

The numerical solution of the function u is given by SSW [7]. The field is apodized with the Hanning window for $z > Z$. In order to compute the adjoint field w, $\phi(z)$ is replaced with the difference $u_m(R, z) - u^{obs}(R, z)$ in SSW and backpropagated in the same domain Ω_{N_r, N_z}. The gradient $\nabla_m J_{AM}$ is estimated by (4) with the Simpson's rule of integration.

The observed field $u^{obs}(R, z)$ is synthetically generated using refractivity model m_{opt} and it is sampled at each grid node, $u^{obs}(R, z) \in \mathbb{C}^{N_z}$. The inversion aims at retrieving $m_{opt} \in \mathbb{R}^{N_z}$ from an initial guess $m_0 \in \mathbb{R}^{N_z}$. The solution m_{opt} can be estimated with a line-search algoritm. The iterations of parameters m can be formulated as:

$$m_{i+1} = m_i - \rho_i \nabla_{m_i} J, \tag{5}$$

where the index i denotes the number of iterations, m_i is the parameter of the i^{th} iteration, $\rho_i = \rho\alpha^b$ and $\nabla_m J_i$ are the stepsize and the gradient of the i^{th} iteration respectively. The parameter b is defined as the smallest integer such that:

$$J\left(m_i - \rho\alpha^b \nabla_{m_i} J\right) < J(m_i), \tag{6}$$

where $\rho = 10^{-4}$ and $\alpha = 0.5$. The stopping criterion of the optimization algorithm is given by:

$$\frac{||m_{i+1} - m_i||}{1 + ||m_0||} \leq 10^{-11}, \tag{7}$$

otherwise a maximum number of iterations of 400 is imposed.

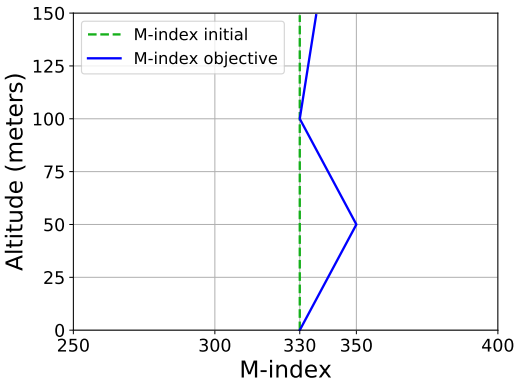

Fig. 2. Initial guess and objective refractivity profile.

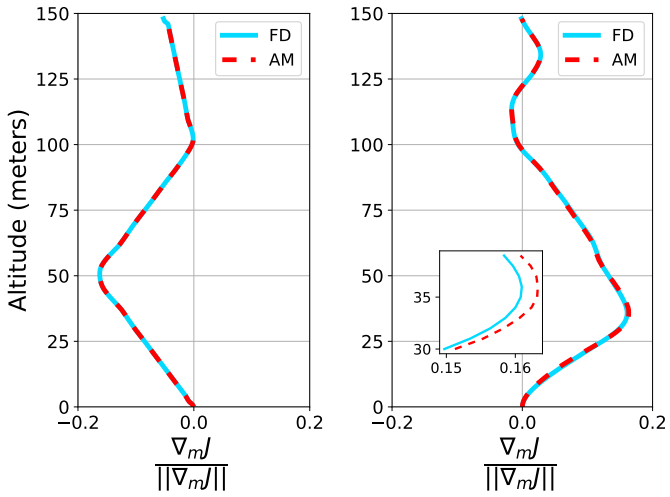

(a) $R = 100$ m. (b) $R = 60$ km.

Fig. 3. Gradients estimated with the finite differences (FD) and the adjoint model (AM) for different range R. The curves follow the synoptic structure of each other.

B. Method of Validation

FD computations can validate AM in different ways [8]. In this work, we use the validation through comparison of the synoptic structure of the gradients $\nabla_m J_{AM}$ and $\nabla_m J_{FD}$. If the adjoint field is formulated and simulated properly, the gradients $\nabla_m J_{AM}$ and $\nabla_m J_{FD}$ should follow each other.

Inspired from [6], a short range propagation setup is organized for the validation purpose. Both gradients are estimated for the parameters given in Fig. 2. The gradient $\nabla_m J_{AM}$ is compared to $\nabla_m J_{FD}$ which is obtained using forward difference scheme for perturbation tolerance $\epsilon = 10^{-7}$ following [8] (Other values of ϵ have been tested. No significant dependence is observed).

In this work, the operator Q^* in (3) is assumed to be self-adjoint ($Q^* \equiv Q$) and the operator Q^{-1^*} in (4) is assumed to approximate to unity ($Q^{-1^*} \equiv 1$). The proof of validity is kept out of scope of this article. However, the numerical tests support the assumptions.

The initial condition $\phi(z)$ is obtained from a complex-point source positioned far from the domain, at $r_s = -100$ km. This is necessary in order to illuminate the duct so that the gradient can be computed for $0 < z < Z$ entirely in short range.

C. Validation

The gradient $\nabla_m J_{AM}$ is compared to $\nabla_m J_{FD}$ in Fig. 3. The curves are normalized by the norm of the gradient. From Fig. 3a, one observes that the gradients of the two different methods follow each other for $R = 100$ m.

The relationship between the m and J is weakly nonlinear in short range. This is confirmed with that $\nabla_m J_{AM}$ in Fig. 3a has a symmetric synoptic structure of $M_{opt} - M_0$ deduced from Fig. 2. To detail, from the gradient $\nabla_m J_{AM}$ being the lowest at $z = 50$ m to its decrease towards null at $z = 100$ m, and the symmetry of the gradient around $z = 50$ m in the range $0 < z < 100$ m are among other things to defend this assertation. Therefore the inversion does not have strong dependence on the initial guess in this scenario.

Increasing nonlinearity of the problem with range impacts on the gradient $\nabla_m J_{AM}$. To illustrate this, the range is increased to $R = 60$ km with cell size to $\Delta r = 100$ m and corresponding $\nabla_m J_{AM}$ is displayed in Fig. 3b. Increasing the range from 100 m to 60 km changes the direction of the gradient $\nabla_m J_{AM}$ mainly to the opposite of that of $R = 100$ m. The fact that $\nabla_m J_{AM}$ is positive at some altitudes does not seem to be in accord with the refractivity parameters (of a weakly nonlinear problem). To remove the doubts on the accuracy of $\nabla_m J_{AM}$, validation with FD is performed again. As depicted in Fig. 3b, both methods estimate the gradient comparably so the assumptions on the adjoint model are validated for long range as well. Having different $\nabla_m J_{AM}$ for different propagation ranges is linked to the high nonlinearity of the problem.

The change of the gradient with increasing nonlinearity (with range) is attributed to the change in driver of the adjoint given with (3b). Consequently, increasing the range impacts on the structure of the adjoint field w which is used for estimating $\nabla_m J_{AM}$ with (4). Let us first consider the case for $R = 100$ m. Fig. 4a shows the adjoint field w obtained by propagating the difference given in Fig. 4b at $r = R$. From Fig. 4b one observes that the difference $|u - u_{obs}|$ is low in short range and its vertical distribution seems to be self-similar with range. This monotonicity with range is observed to ensure $|u - u_{obs}| = 0$ at the altitude $z = 100$ m following $(M_{opt} - M_0)|_{z=100\ \mathrm{m}} = 0$. However, the nonlinearity between m and J gets severe with range and the gradient progressively deviates from that given in Fig. 3a. This is linked to the emergence of new local minima; the gradient points towards the nearest minimum. This is supported by the increasing nonlinearity of $|u - u_{obs}|$ which is obvious for increasing ranges in Fig. 5b. Thus, one expects to lose track of the global minimum as propagation range increases. Note that the objective duct is an oversimplified example of what is encountered in reality, still the inversions are expected to suffer from nonlinearity beyond 5-6 km range. Finally, the adjoint w

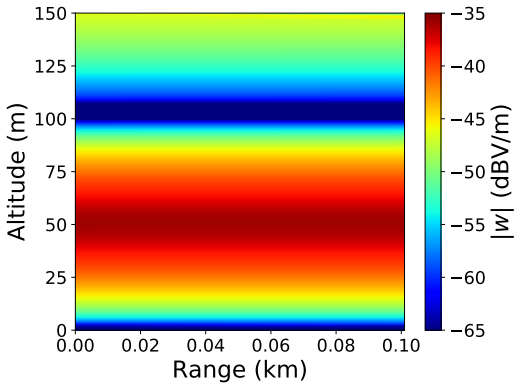

(a)

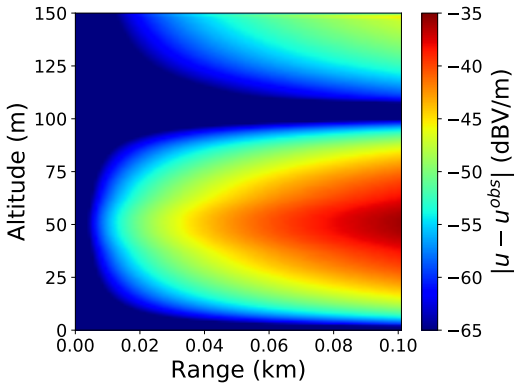

(b)

Fig. 4. For propagation range $R = 100$ m, (a) backpropagation of the adjoint field w (dBV/m), (b) the difference between the initial guess field u (dBV/m) and the observation u^{obs} (dBV/m).

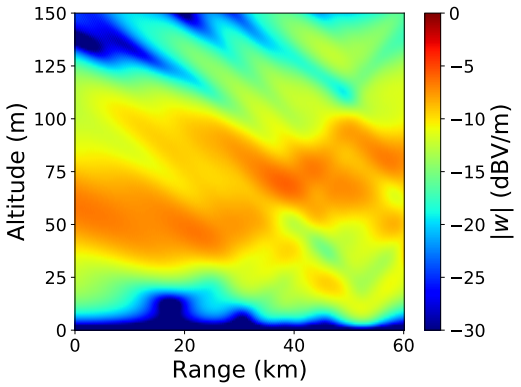

(a)

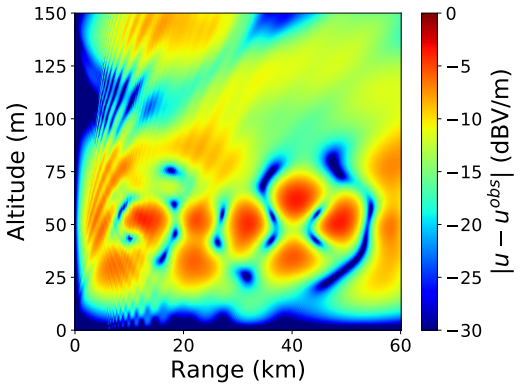

(b)

Fig. 5. For propagation range $R = 60$ km, (a) backpropagation of the adjoint field w (dBV/m), (b) the difference between the initial guess field u (dBV/m) and the observation u^{obs} (dBV/m).

for $R = 60$ km is presented in Fig. 5a for completeness of the discussion. Comparison between Fig. 4a and Fig. 5a shows an example of how different the error $u_m(R, z) - u^{obs}(R, z)$ back-propagates for different degrees of nonlinearity. Accordingly, $\nabla_m J_{AM}$ depends on the range of propagation.

To summarize, the adjoint model is validated and non-linearity of the problem is elaborated. Given the degree of nonlinearity of an oversimplified case, an accurate RFC system has to consider mitigation of nonlinearity as a second step, following the validation of the gradient.

D. Inversion Results

We test our method of inversion in order to prove that the inversion strategy is implemented properly. The objective duct is given in Fig. 2. The computational setup of the inversion is given in section IV-A.

In short ranges the convergence of the inversion is seen from the decrease of the cost function with iterations in Fig. 6a. The inversion has converged after 131 iterations. The success of the inversion is seen from the match between initial and objective modified refractivity profiles in Fig. 6b.

The inversion parameters m_{inv} capture most of the objective duct profile given by m_{opt} in only the first two iterations. This is achieved thanks to not only the accuracy of the method to compute the gradient but also the assist of the weak nonlinearity. From 2^{nd} to 8^{th} iterations, the effort is mostly dedicated to the capturing of the abrupt variation of m_{opt} around $z = 50$ m. The abrupt variation is not perfectly captured in the gradient (see Fig. 3a) partly due to the physical diffusion in (1) and (3). However it is not associated with the assumptions on the operator Q because FD predicts the gradient comparably smooth. This is an example of common difficulty to capture abrupt variations in nonlinear inverse problems. We note that the remaining 123 iterations are performed mainly so as to smoothen the oscillations of m_{inv} around m_{opt}. These oscillations spread over m_{inv} during iterations and they originate from the abrupt variation of m_{opt} at $z = 50$ m. The convergence can be improved by convexifying the cost function with the application of regularization techniques. However, one anticipates that the improvement of convergence rate at the level of these oscillations are not a concern when noise is introduced in realistic scenarios as the cost function remains higher than it is beyond 8^{th} iteration in Fig. 6a.

As for the case with $R = 60$ km, the inversion is not successful. Convergence criterion is not met until maximum

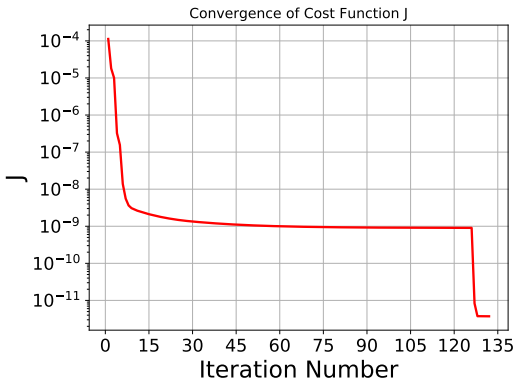

(a)

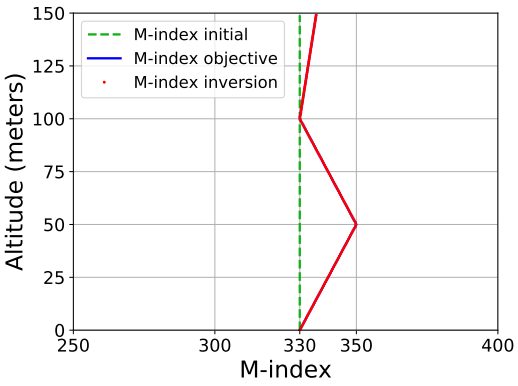

(b)

Fig. 6. For propagation range $R = 100$ m, (a) convergence plot, (b) the initial guess, objective and inverted modified refractivity.

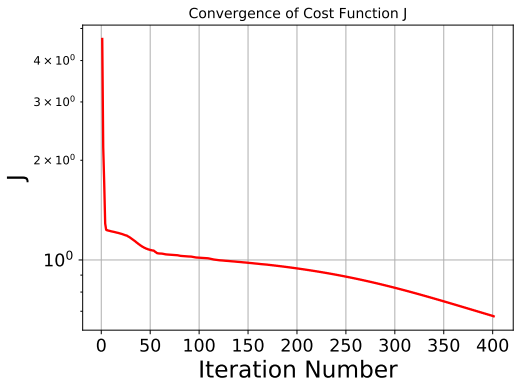

(a)

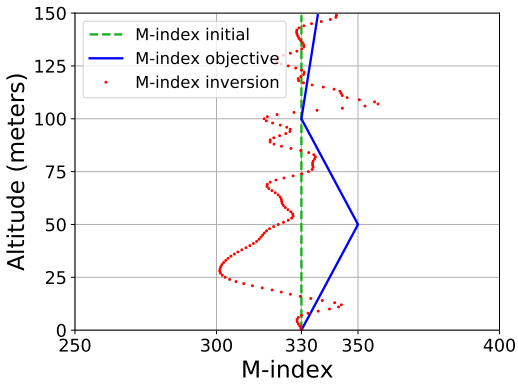

(b)

Fig. 7. For propagation range $R = 60$ km, (a) convergence plot, (b) the initial guess, objective and inverted modified refractivity.

allowed 400 iterations. The inverted refractivity parameters do not follow the objective in Fig. 7b. The failure is owing to the nonlinearity of the problem; the inversion converges at the minimum which is the nearest to the given initial condition. Rate of convergence is also slower than that of $R = 100$ m in Fig. 7a. Mitigation of nonlinearity is mandatory for a successful inversion because a good initial guess is typically unavailable.

V. Conclusion

The adjoint model for a wide-angle parabolic equation has been introduced. The numerical solution of the new adjoint formulation using SSW has been validated with the method of finite differences. Inversions are succesful only in short range propagation. The nonlinear problem requires mitigation of nonlinearity to successfully invert in long range.

In future work, we will aim at improving our results by combining multiscale parametrization [9] and different regularization methods [8]. More realistic ducts will be analysed and robustness tests with respect to noise will be executed.

Acknowledgment

This work is part of activities of ENAC/ISAE-SUPAERO/ONERA Research Federation.

References

[1] C. Yardim, "Statistical estimation and tracking of refractivity from radar clutter," Ph.D. dissertation, UC San Diego, 2007.

[2] R. Douvenot and V. Fabbro, "On the knowledge of radar coverage at sea using real time refractivity from clutter," *IET radar, sonar & navigation*, vol. 4, pp. 293–301, 2010.

[3] A. Karimian, C. Yardim, P. Gerstoft, W. S. Hodgkiss, and A. E. Barrios, "Refractivity estimation from sea clutter: An invited review," *Radio Science*, vol. 46, pp. 1–16, 2011.

[4] M. A. Gilles, C. Earls, and D. Bindel, "A subspace pursuit method to infer refractivity in the marine atmospheric boundary layer," *IEEE Transactions on Geoscience and Remote Sensing*, vol. 57, pp. 5606–5617, 2019.

[5] D. Dockery and J. R. Kuttler, "An improved impedance-boundary algorithm for fourier split-step solutions of the parabolic wave equation," *IEEE Transactions on Antennas and Propagation*, vol. 44, no. 12, pp. 1592–1599, 1996.

[6] X.-F. Zhao, S.-X. Huang, and H.-D. Du, "Theoretical analysis and numerical experiments of variational adjoint approach for refractivity estimation," *Radio Science*, vol. 46, 2011.

[7] H. Zhou, R. Douvenot, and A. Chabory, "Modeling the long-range wave propagation by a split-step wavelet method," *Journal of Computational Physics*, in press.

[8] M. Kern, *Numerical Methods for Inverse Problems*. John Wiley & Sons, 2016.

[9] Y. Diouane, S. Gratton, X. Vasseur, L. N. Vicente, and H. Calandra, "A parallel evolution strategy for an earth imaging problem in geophysics," *Optimization and Engineering*, vol. 17, no. 1, pp. 3–26, 2016.